Ain Shams Engineering Journal (2013) 4, 879–888

Ain Shams University

Ain Shams Engineering Journal

www.elsevier.com/locate/asej
www.sciencedirect.com

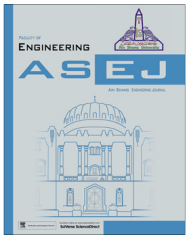

MECHANICAL ENGINEERING

Chemically reactive species and radiation effects on MHD convective flow past a moving vertical cylinder

Gnaneswara Reddy Machireddy *

Department of Mathematics, Acharya Nagarjuna University Ongole Campus, Ongole, AP 523 001, India

Received 14 November 2012; revised 2 April 2013; accepted 11 April 2013
Available online 22 May 2013

KEYWORDS

Radiation;
MHD;
Chemically reactive species;
Finite difference scheme;
Vertical cylinder

Abstract The numerical solution of transient natural convection flow of radiation effects on MHD heat and mass transfer past a moving vertical cylinder with chemical reaction is presented. The governing boundary layer equations for the above flow problem of first-order homogeneous chemical reaction are setup and non-dimensionalized. An implicit finite difference method is used to solve the unsteady, non-linear, and coupled governing equations. Numerical results are presented for various parameters. The unsteady velocity, temperature, concentration profiles, local and average skin-friction, Nusselt number, and Sherwood number are shown graphically and are discussed for both generative and destructive reaction.

1. Introduction

Natural convection flows are frequently encountered in nature. They have wide applications in Science and Technology. These types of problems are commonly encountered in start-up of a chemical reactor and emergency cooling of a nuclear fuel element. In the case of power or pump failure, similar conditions may arise for devices cooled by forced circulation, as in the core of a nuclear reactor. In the glass and polymer industries, hot filaments, which are considered as a vertical cylinder, are cooled as they pass through the surrounding environment. The analytical methods fail to solve the problems of unsteady natural convection flows past a semi-infinite vertical cylinder. The advanced numerical methods and computer technology have shown the way in which such difficult problems can be solved. Finite difference methods play a major role in solving partial differential equations. Several investigators under different boundary conditions have analyzed steady free convection along vertical cylinders. The study of unsteady boundary layer flow over a moving vertical cylinder has important geophysical and engineering applications. For example, as a result of volcanic activities or tectonic movements, magmatic intrusion may occur at shallow depths in the earth's crust. The intrusive magma may take the form of a cylindrical shape. An experimental and analytical study is reported by Evan et al. [1] for transient natural convection in a vertical cylinder. Velusamy and Grag [2] given a numerical solution for the transient natural convection over a heat generating vertical cylinder.

The study of flow problems, which involve the interaction of several phenomena, has a wide range of applications in the field of science and technology. One such study is related

* Tel.: +91 9490636769; fax: +91 08592224842.
E-mail address: mgrmaths@gmail.com.

Peer review under responsibility of Ain Shams University.

ELSEVIER Production and hosting by Elsevier

2090-4479 © 2013 Ain Shams University. Production and hosting by Elsevier B.V. All rights reserved.
http://dx.doi.org/10.1016/j.asej.2013.04.003

Nomenclature

B_0	magnetic field strength
C'	species concentration
C	dimensionless species concentration
D	the species diffusion coefficient
Gr	thermal Grashof number
Gc	modified Grashof number
g	acceleration due to gravity
i	grid point along the X – direction
j	grid point along the R – direction
k_1	chemical reaction parameter
K	dimensionless chemical reaction parameter
M	magnetic parameter
N	radiation parameter
$\overline{Nu}$	average Nusselt number
Nu_x	local Nusselt number
Pr	Prandtl number
q_r	radiative heat flux
R	dimensionless radial co-ordinate
r	radical co-ordinate
r_0	radius of cylinder
Sc	Schmidt number
$\overline{Sh}$	average Sherwood number
Sh_X	local Sherwood number
T	temperature
t	time
X	dimensionless axial co-ordinate
U,V	dimensionless velocity components in X, R directions respectively

Greek symbols

α	thermal diffusivity
β	volumetric coefficient of thermal expansion
β^*	volumetric coefficient of expansion with concentration
Δt	grid size in time
ΔR	grid size in radical direction
ΔX	grid size in axial direction
k_e	mean absorption coefficient
ν	kinematic viscosity
ρ	density
σ_s	Stefan–Boltzmann constant
τ_x	local skin-friction
$\bar{\tau}$	average skin-friction

Subscripts

w	condition on the wall
∞	free-stream condition

to the effects of free convection MHD flow, which plays an important role in agriculture, engineering, and petroleum industries. The problem of free convection under the influence of a magnetic field has attracted the interest of many researchers in view of its application in geophysics and in astrophysics. The problem under consideration has important applications in the study of geological formations; in the exploration and thermal recovery of oil; and in the assessment of aquifers, geothermal reservoirs, and underground nuclear waste storage sites. Results obtained from this study will be helpful in the prediction of flow, heat transfer, and solute or contaminant dispersion about intrusive bodies such as salt domes, magnetic intrusions, piping, and casting systems. Michiyoshi et al. [3] considered natural convection heat transfer from a horizontal cylinder to mercury under a magnetic field. Magnetic field effect on a moving vertical cylinder with constant heat flux was given by Ganesan and Loganathan [4]. Gnaneswara Reddy et al. [5] presented unsteady MHD convective heat and mass transfer flow past a semi-infinite vertical porous plate with variable viscosity and thermal conductivity.

Free convection flow involving coupled heat and mass transfer occurs frequently in nature. It occurs not only due to temperature differences, but also due to concentration differences or a combination of these two, for example, in atmospheric flows there exist differences in the H_2O concentration. A few representative fields of interest in which combined heat and mass transfer plays an important role are designing of chemical processing equipment, formation and dispersion of fog, distribution of temperature and moisture over agricultural fields and groves of fruit trees, crop damage due to freezing, and environmental pollution. The effects of heat and mass transfer on natural convection flow over a vertical cylinder were studied by Chen and Yuh [6]. Combined heat and mass transfer effects on moving vertical cylinder for steady and unsteady flows were analyzed by Takhar et al. [7] and Ganesan and Loganathan [8], respectively. A numerical solution for the transient natural convection flow over a vertical cylinder under the combined buoyancy effect of heat and mass transfer was given by Ganesan and Rani [9], by employing an implicit finite difference scheme. Shanker and Kishan [10] presented the effect of mass transfer on the MHD flow past an impulsively started infinite vertical plate. Ganesan and Rani [11] studied the MHD unsteady free convection flow past a vertical cylinder with heat and mass transfer. Gnaneswara Reddy [12] has analyzed unsteady free convective flow past a semi-infinite vertical plate with uniform heat and mass flux.

In the context of space technology and in processes involving high temperatures, the effects of radiation are of vital importance. Studies of free convection flow along a vertical cylinder or horizontal cylinder are important in the field of geothermal power generation and drilling operations where the free stream and buoyancy induced fluid velocities are of roughly the same order of magnitude. Many researchers such as Arpaci [13], Cess [14], Cheng and Ozisik [15], Raptis [16], Hossain, and Takhar [17,18] have investigated the interaction of thermal radiation and free convection for different geometries, by considering the flow to be steady. The unsteady flow past a moving vertical plate in the presence of free convection and radiation were studied by Das et al. [19]. The combined radiation and free convection flow over a vertical cylinder was studied by Yih [20]. Radiation and mass transfer effects on flow of an incompressible viscous fluid past a moving vertical cylinder was studied by Ganesan and Loganathan [21]. Very recently, Gnaneswara Reddy and Bhaskar Reddy [22]

presented the radiation and mass transfer effects on unsteady MHD free convection flow past a moving vertical cylinder. Thermal radiation and mass transfer effects on MHD free convection flow past a vertical cylinder with variable surface temperature and concentration presented by Gnaneswara Reddy and Bhaskar Reddy [23]. The chemically reacting hydromagnetic unsteady flow of a radiating fluid past a vertical plate is studied by Makinde [24,25]. Ibrahim and Makinde [26] considered Radiation Effect on Chemically Reacting MHD Boundary Layer Flow of Heat and Mass Transfer Past a Porous Vertical flat Plate.

The unsteady natural convection MHD radiating fluid flow over a moving vertical cylinder with chemical reaction has given very scant attention in literature. Hence, the objective of this paper is to study the radiation and mass transfer effects on hydromagnetic free convection flow of a viscous incompressible optically thick fluid past a moving vertical cylinder. Here, we assume that a chemically reactive species is emitted from the surface of the cylinder and diffuses into the fluid. The reaction is assumed to take place entirely in the stream. In the present study, the concentration distribution of this particular component in the flow filed is calculated. No analysis seems to have been presented for transient natural convection along vertical cylinders under uniform temperature/concentration along with chemical reaction. The main reason for the lack of study of this problem is due to difficult mathematical and numerical procedures in dealing with the non-similar boundary layers. Due to the importance of this study in many applications, the present study is attempted. The conservation equations of an unsteady laminar boundary layer are first transformed into a non-dimensional form and their solutions are then obtained by an efficient implicit finite difference scheme of Crank–Nicolson type. The behavior of the velocity, temperature, concentration, skin-friction, Nusselt number, and Sherwood number has been discussed for variations in the governing thermophysical and hydrodynamical parameters.

2. Mathematical analysis

Consider a two-dimensional unsteady free convection flow of a viscous incompressible electrically conducting and radiating optically thick fluid past an impulsively started semi-infinite vertical cylinder of radius r_0. The physical model of the analysis is shown in Fig. 1. Here, the x-axis is taken along the axis of cylinder in the vertical direction and the radial coordinate r is taken normal to the cylinder. Initially, the fluid and the cylinder are at the same temperature T'_∞ and the concentration C'_∞. At time $t' > 0$, the cylinder starts moving in the vertical direction with velocity u_0 and the surface of the cylinder is raised to a uniform temperature T'_w and concentration C'_w and are maintained constantly thereafter. A uniform magnetic field is applied in the direction perpendicular to the cylinder. The fluid is assumed to be slightly conducting, and hence, the magnetic Reynolds number is much less than unity and the induced magnetic field is negligible in comparison with the applied magnetic field. It is further assumed that there is no applied voltage, so that electric field is absent. It is also assumed that the radiative heat flux in the x-direction is negligible as compared to that in the radial direction. The viscous dissipation is also assumed to be negligible in the energy equation due to slow motion of the cylinder. It is also assumed that there exists a homogeneous first order chemical reaction between the fluid and species concentration. But here we assume the level of species concentration to be very low and hence heat generated during chemical reaction can be neglected. In this reaction, the reactive component given off by the surface occurs only in very dilute form. Hence, any convective mass transport to or from the surface due to a net Viscous dissipation effects in the energy equation are assumed to be negligible. It is also assumed that all the fluid properties are constant except that of the influence of the density variation with temperature and concentration in the body force term (Boussinesq's approximation). The foreign mass present in the flow is assumed to be at low level, and hence, Soret and Dufour effects are negligible.

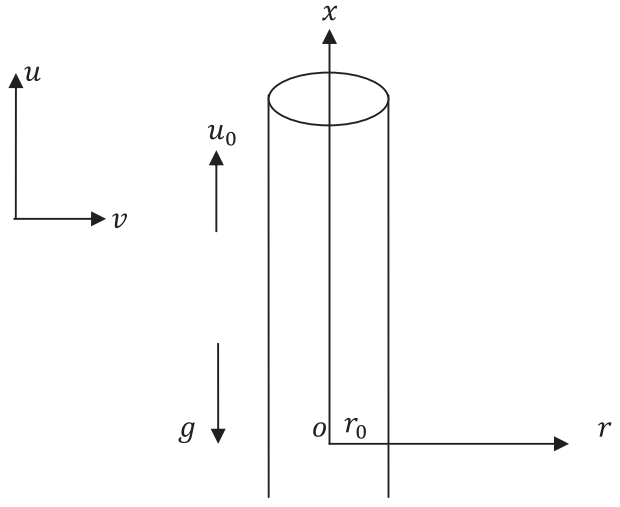

Figure 1 The physical model and coordinate system.

Then, the flow under consideration is governed by the following system of equations:

Continuity equation

$$\frac{\partial(ru)}{\partial x}+\frac{\partial(r)}{\partial r}=0 \tag{1}$$

Momentum equation

$$\frac{\partial u}{\partial t'}+u\frac{\partial u}{\partial x}+\frac{\partial u}{\partial r}=g\beta(T'-T'_\infty)+g\beta^*(C'-C'_\infty)+\frac{v}{r}\times\frac{\partial}{\partial r}\left(r\frac{\partial u}{\partial r}\right)-\frac{\sigma B_0^2}{\rho}u \tag{2}$$

Energy equation

$$\frac{\partial T'}{\partial t'}+u\frac{\partial T'}{\partial x}+\frac{\partial T'}{\partial r}=\frac{\alpha}{r}\frac{\partial}{\partial r}\left(r\frac{\partial T'}{\partial r}\right)-\frac{1}{\rho c_p}\frac{1}{r}\frac{\partial}{\partial r}(rq_r) \tag{3}$$

Mass diffusion equation

$$\frac{\partial C'}{\partial t'}+u\frac{\partial C'}{\partial x}+\frac{\partial C'}{\partial r}=\frac{D}{r}\frac{\partial}{\partial r}\left(r\frac{\partial C'}{\partial r}\right)-k_1C' \tag{4}$$

The initial and boundary conditions are:

$$\begin{aligned}
&t'\leqslant 0: u=0,=0, T'=T'_\infty, C'=C'_\infty \quad \text{for all } x\geqslant 0 \text{ and } r\geqslant 0\\
&t'>0: u=u_0,=0, T'=T'_w, C'=C'_w \quad \text{at } r=r_0\\
&\qquad u=0,=0, T'=T'_\infty, C'=C'_\infty \quad \text{at } x=0 \text{ and } r\geqslant r_0\\
&\qquad u\to 0, T'\to T'_\infty, C'\to C'_\infty \quad \text{as } r\to\infty
\end{aligned} \tag{5}$$

By using the Rosseland approximation (Brewster [27]), the radiative heat flux q_r is given by

$$q_r = -\frac{4\sigma_s}{3k_e}\frac{\partial T'^4}{\partial r} \tag{6}$$

where σ_s is the Stefan–Boltzmann constant and k_e is the mean absorption coefficient. It should be noted that by using the Rosseland approximation, the present analysis is limited to optically thick fluids. If the temperature differences within the flow are sufficiently small, then Eq. (6) can be linearized by expanding T'^4 into the Taylor series about T'_∞, which after neglecting higher order terms takes the form:

$$T'^4 \cong 4T'^3_\infty T' - 3T'^4_\infty \tag{7}$$

In view of Eqs. (6) and (7), Eq. (3) reduces to

$$\frac{\partial T'}{\partial t'} + u\frac{\partial T'}{\partial x} + \frac{\partial T'}{\partial r} = \frac{\alpha}{r}\frac{\partial}{\partial r}\left(r\frac{\partial T'}{\partial r}\right) + \frac{16\sigma_s T'^3_\infty}{3k_e\rho c_p}\frac{1}{r} \times \frac{\partial}{\partial r}\left(r\frac{\partial T'}{\partial r}\right) \tag{8}$$

Knowing the velocity, temperature and concentration fields, it is interesting to study the local and average skin-frictions, Nusselt numbers and Sherwood numbers, which are defined as follows.

Local and average skin-frictions are given respectively by:

$$\tau'_x = -\mu\left(\frac{\partial u}{\partial r}\right)_{r=r_0} \tag{9}$$

$$\overline{\tau}_L = \frac{-1}{L}\int_0^L \mu\left(\frac{\partial u}{\partial r}\right)_{r=r_0} dx \tag{10}$$

Local and average Nusselt numbers are given respectively by

$$Nu_x = \frac{-x\left(\frac{\partial T'}{\partial r}\right)_{r=r_0}}{T'_w - T'_\infty} \tag{11}$$

$$\overline{Nu}_L = -\int_0^L \left[\left(\frac{\partial T'}{\partial r}\right)_{r=r_0} \Big/ (T'_w - T'_\infty)\right] dx \tag{12}$$

Local and average Sherwood numbers are given respectively by:

$$Sh_x = \frac{-x\left(\frac{\partial C'}{\partial r}\right)_{r=r_0}}{C'_w - C'_\infty} \tag{13}$$

$$\overline{Sh}_L = -\int_0^L \left[\left(\frac{\partial C'}{\partial r}\right)_{r=r_0} \Big/ (C'_w - C'_\infty)\right] dx \tag{14}$$

In order to write the governing equations and the boundary conditions in dimensionless form, the following non-dimensional quantities are introduced.

$$X = \frac{xv}{u_0 r_0^2},\quad R = \frac{r}{r_0},\quad t = \frac{t'v}{r_0^2},\quad U = \frac{u}{u_0},\quad V = \frac{r_0}{v},\quad Gr = \frac{g\beta r_0^2(T'_w - T'_\infty)}{vu_0}$$
$$Gc = \frac{g\beta^* r_0^2(C'_w - C'_\infty)}{vu_0},\quad N = \frac{k_e k}{4\sigma_s T'^3_\infty},\quad M = \frac{\sigma B_0^2 r_0^2}{\rho v},\quad T = \frac{T' - T'_\infty}{T'_w - T'_\infty},$$
$$C = \frac{C' - C'_\infty}{C'_w - C'_\infty},\quad Pr = \frac{v}{\alpha},\quad Sc = \frac{v}{D},\quad K = \frac{k_1 r_0^2}{v} \tag{15}$$

In view of the Eq. (15), the Eqs. (1), (2), (8), and (4) reduce to the following non-dimensional form:

$$\frac{\partial(\mathrm{RU})}{\partial X} + \frac{\partial(\mathrm{RV})}{\partial R} = 0 \tag{16}$$

$$\frac{\partial U}{\partial t} + U\frac{\partial U}{\partial X} + V\frac{\partial U}{\partial R} = GrT + GcC + \frac{1}{R}\frac{\partial}{\partial R}\left(R\frac{\partial U}{\partial R}\right) - \mathrm{MU} \tag{17}$$

$$\frac{\partial T}{\partial t} + U\frac{\partial T}{\partial X} + V\frac{\partial T}{\partial R} = \frac{1}{Pr}\left(1 + \frac{4}{3N}\right)\frac{1}{R}\frac{\partial}{\partial R}\left(R\frac{\partial T}{\partial R}\right) \tag{18}$$

$$\frac{\partial C}{\partial t} + U\frac{\partial C}{\partial X} + V\frac{\partial C}{\partial R} = \frac{1}{Sc}\frac{1}{\partial R}\left(R\frac{\partial C}{\partial R}\right) - \mathrm{KC} \tag{19}$$

The corresponding initial and boundary conditions are:

$$\begin{aligned} &t \leqslant 0 : U = 0, V = 0, T = 0, C = 0 \quad \text{for all } X \geqslant 0 \text{ and } R \geqslant 0 \\ &t > 0 : U = 1, V = 0, T = 1, C = 1 \quad \text{at } (R = 1) \\ &\qquad U = 0, T = 0, C = 0 \quad \text{at } X = 0 \text{ and } R \geqslant 1 \\ &\qquad U \to 0, T \to 0, C \to 0 \quad \text{as } R \to \infty \end{aligned} \tag{20}$$

where Gr is the thermal Grashof number, Gc the solutal Grashof number, M the magnetic parameter, Pr the Prandtl number, N the radiation parameter and Sc the Schmidt number, and K is the chemical reaction parameter.

Local and average skin-frictions in non-dimensional form are given by:

$$\tau_X = -\left(\frac{\partial U}{\partial R}\right)_{R=1} \tag{21}$$

$$\overline{\tau} = -\int_0^1 \left(\frac{\partial U}{\partial R}\right)_{R=1} dX \tag{22}$$

Local and average Nusselt numbers in non-dimensional form are given by:

$$Nu_X = -X\left(\frac{\partial T}{\partial R}\right)_{R=1} \tag{23}$$

$$\overline{Nu} = -\int_0^1 \left(\frac{\partial T}{\partial R}\right)_{R=1} dX \tag{24}$$

Local and average Sherwood numbers in non-dimensional form are given by:

$$Sh_X = -X\left(\frac{\partial C}{\partial R}\right)_{R=1} \tag{25}$$

$$\overline{Sh} = -\int_0^1 \left(\frac{\partial C}{\partial R}\right)_{R=1} dX \tag{26}$$

3. Numerical technique

In order to solve the unsteady, non-linear coupled Eqs. (16)–(19) under the conditions (20), an implicit finite difference scheme of Crank–Nicolson type has been employed. The region of integration is considered as a rectangle with sides $X_{\max}$ (= 1) and $R_{\max}$ (= 14), where $R_{\max}$ corresponds to $R = \infty$, which lies very well outside the momentum, energy, and con-

centration boundary layers. The maximum of R was chosen as 14 after some preliminary investigations, so that the last two of the boundary conditions (20) are satisfied within the tolerance limit 10^{-5}. The grid system is shown in the following figure.

The finite difference equations corresponding to Eqs. (16)–(19) are as follows.

$$\frac{[U_{i,j}^{n+1}-U_{i-1,j}^{n+1}+U_{i,j}^{n}-U_{i-1,j}^{n}+U_{i,j-1}^{n+1}-U_{i-1,j-1}^{n+1}+U_{i,j-1}^{n}-U_{i-1,j-1}^{n}]}{4\Delta X}+\frac{[V_{i,j}^{n+1}-V_{i,j-1}^{n+1}+V_{i,j}^{n}-V_{i,j-1}^{n}]}{2\Delta R}+\frac{V_{i,j}^{n+1}}{1+(j-1)\Delta R}=0 \tag{27}$$

$$\begin{aligned}&\frac{[U_{i,j}^{n+1}-U_{i,j}^{n}]}{\Delta t}+U_{i,j}^{n}\frac{[U_{i,j}^{n+1}-U_{i-1,j}^{n+1}+U_{i,j}^{n}-U_{i-1,j}^{n}]}{2\Delta X}+V_{i,j}^{n}\\&\times\frac{[U_{i,j+1}^{n+1}-U_{i,j-1}^{n+1}+U_{i,j+1}^{n}-U_{i,j-1}^{n}]}{4\Delta R}\\&=Gr\frac{[T_{i,j}^{n+1}+T_{i,j}^{n}]}{2}+Gc\frac{[C_{i,j}^{n+1}+C_{i,j}^{n}]}{2}\\&\quad+\frac{[U_{i,j-1}^{n+1}-2U_{ij}^{n+1}+U_{i,j+1}^{n+1}+U_{i,j+1}^{n+1}-2U_{i,j}^{n}+U_{i,j+1}^{n}]}{2(\Delta R)^2}\\&\quad+\frac{[U_{i,j+1}^{n+1}-U_{i,j-1}^{n+1}+U_{i,j+1}^{n}-U_{i,j-1}^{n}]}{4[1+(j-1)\Delta R]\Delta R}-\frac{M}{2}[U_{i,j}^{n+1}+U_{i,j}^{n}]\end{aligned} \tag{28}$$

$$\begin{aligned}&\frac{[T_{i,j}^{n+1}-T_{i,j}^{n}]}{\Delta t}+U_{i,j}^{n}\frac{[T_{i,j}^{n+1}-T_{i-1,j}^{n+1}+T_{i,j}^{n}-T_{i-1,j}^{n}]}{2\Delta X}\\&+V_{i,j}^{n}\frac{[T_{i,j+1}^{n+1}-T_{i,j-1}^{n+1}+T_{i,j+1}^{n}-T_{i,j-1}^{n}]}{4\Delta R}\\&=\frac{1}{Pr}\left(1+\frac{4}{3N}\right)\left(\frac{[T_{i,j-1}^{n+1}-2T_{i,j}^{n+1}+T_{i,j+1}^{n+1}+T_{i,j-1}^{n}-2T_{i,j}^{n}+T_{i,j+1}^{n}]}{2(\Delta R)^2}\right.\\&\left.+\frac{[T_{i,j+1}^{n+1}-T_{i,j-1}^{n+1}+T_{i,j+1}^{n}-T_{i,j-1}^{n}]}{4[1+(j-1)\Delta R]\Delta R}\right)\end{aligned} \tag{29}$$

$$\begin{aligned}&\frac{[C_{i,j}^{n+1}-C_{i,j}^{n}]}{\Delta t}+U_{i,j}^{n}\frac{[C_{i,j}^{n+1}-C_{i-1,j}^{n+1}+C_{i,j}^{n}-C_{i-1,j}^{n}]}{2\Delta X}+V_{i,j}^{n}\\&\times\frac{[C_{i,j+1}^{n+1}-C_{i,j-1}^{n+1}+C_{i,j+1}^{n}-C_{i,j-1}^{n}]}{4\Delta R}\\&=\frac{1}{Sc}\frac{[C_{i,j-1}^{n+1}-2C_{i,j}^{n+1}+C_{i,j+1}^{n+1}+C_{i,j-1}^{n}-2C_{i,j}^{n}+C_{i,j+1}^{n}]}{2(\Delta R)^2}\\&\quad+\frac{[C_{i,j+1}^{n+1}-C_{i,j-1}^{n+1}+C_{i,j+1}^{n}-C_{i,j-1}^{n}]}{4Sc[1+(j-1)\Delta R]\Delta R}-\frac{K}{2}[C_{i,j}^{n+1}+C_{i,j}^{n}]\end{aligned} \tag{30}$$

Here, the subscript i – designates the grid point along the X – direction, j – along the R – direction, and the superscript n along the t – direction. The appropriate mesh sizes considered for the calculation are $\Delta X = 0.05$, $\Delta R = 0.25$, and time step $\Delta t = 0.01$. During any one-time step, the coefficients $U_{i,j}^{n}$ and $V_{i,j}^{n}$ appearing in the difference equations are treated as constants. The values of U, V, T, and CO are known at all grid points at $t = 0$ from the initial conditions. The computations of U, V, T, and C at time level $(n + 1)$ using the known values at previous time level (n) are calculated as follows.

The finite difference Eq. (30) at every internal nodal point on a particular i – level constitutes a tri-diagonal system of equations. Such a system of equations is solved by Thomas algorithm as described in Carnahan et al. [28]. Thus, the values of C are found at every nodal point on a particular i at $(n + 1)$th time level. Similarly, the values of T are calculated from the Eq. (29). Using the values of C and T at $(n + 1)$th time level in the Eq. (28), the values of U at $(n + 1)$th time level are found in a similar manner. Thus, the values of C, $T$and U are known on a particular i – level. The values of V are calculated explicitly using the Eq. (27) at every nodal point on a particular i – level at $(n + 1)$th time level. This process is repeated for various i – levels. Thus, the values of C, T, U, and V are known at all grid points in the rectangular region at $(n + 1)$th time level. Computations are carried out till the steady state is reached. The steady state solution is assumed to have been reached, when the absolute difference between the values of U as well as temperature T and concentration C at two consecutive time steps are less than 10^{-5} at all grid points.

After experimenting with few sets of mesh sizes, they have been fixed at the level $\Delta X = 0.05$, $\Delta R = 0.25$, and the time step $\Delta t = 0.01$. In this case, spatial mesh sizes are reduced by 50% in one direction, and then in both directions, and the results are compared. It is observed that, when the mesh size is reduced by 50% in X – direction and R – direction, the results differ in the fourth decimal places. The computer takes more time to compute, if the size of the time-step is small. Hence, the above mentioned sizes have been considered as appropriate mesh sizes for calculation.

The local truncation error in the finite difference approximation is $O(\Delta t^2 + \Delta R^2 + \Delta X)$ and it tends to zero as ΔX, ΔR, and Δt end to zero. Hence, the scheme is compatible. Stability and compatibility ensures convergence [29].

The derivatives involved in the Eqs. (21)–(26) are evaluated using five-point approximation formula, and the integrals are evaluated using Newton–Cotes closed integration formula.

4. Results and discussion

In order to get a physical insight into the problem, a representative set of numerical results is shown graphically in Figs. 2–15, to illustrate the influence of governing parameters viz., radiation parameter N, thermal Grashof number Gr, solutal Grashof number Gc, magnetic field parameter M, and Schmidt number Sc on the velocity, temperature, and concentration. The value of the Prandtl number Pr is chosen to be 0.71, which corresponds air and the values of Sc are choosen such that they represent water vapor (0.6) and carbon dioxide (0.94).

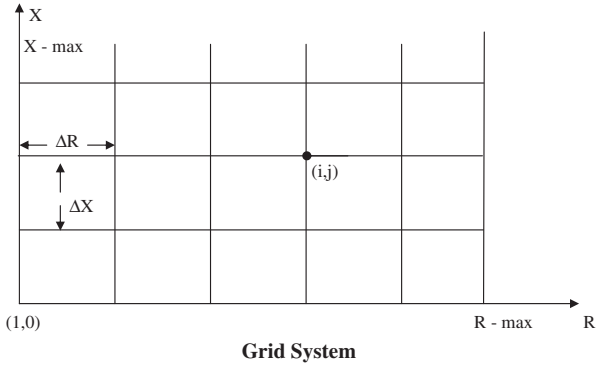

Figure 2 Grid system.

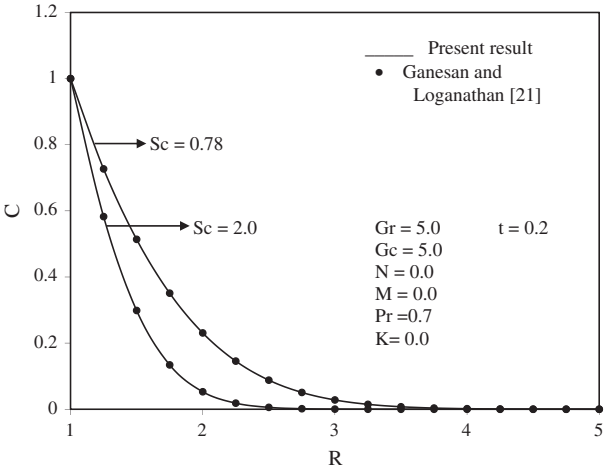

Figure 3 Comparison of concentration profiles.

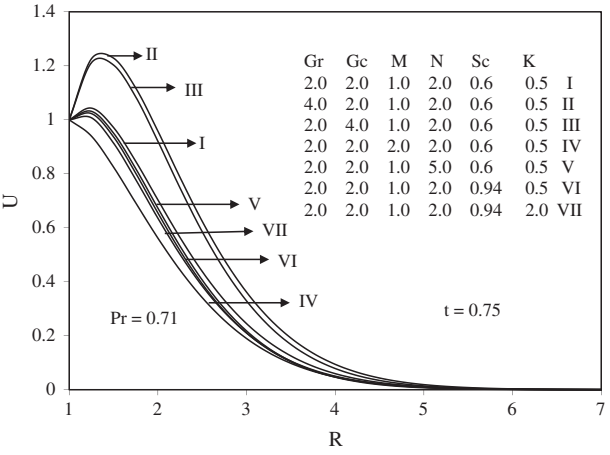

Figure 4 Transient velocity profiles at $X = 1.0$ for different Gr, Gc, M, N, Sc, and K.

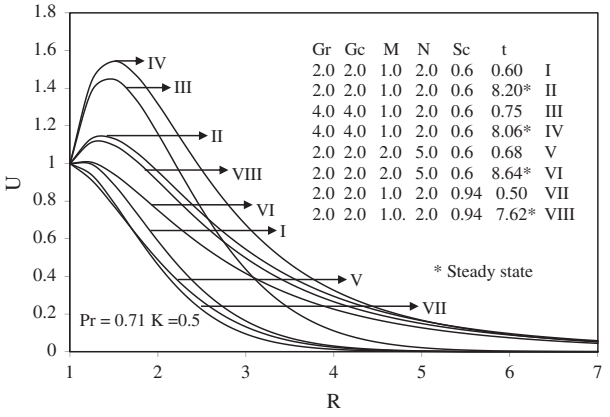

Figure 5 Velocity profiles at $X = 1.0$ for different Gr, Gc, M, N, and Sc.

To validate the current numerical procedure, the present concentration profiles are compared with those of the available isothermal and constant viscosity results of Ganesan and Loganathan [21] for $Gr = 5.0$, $Gc = 5.0$, $N = 0.0$, $M = 0.0$, $Pr = 0.7$, $K = 0.0$, as no experimental or analytical studies exist for the present problem. The comparison results, which are shown in Fig. 3, are found to be in good agreement.

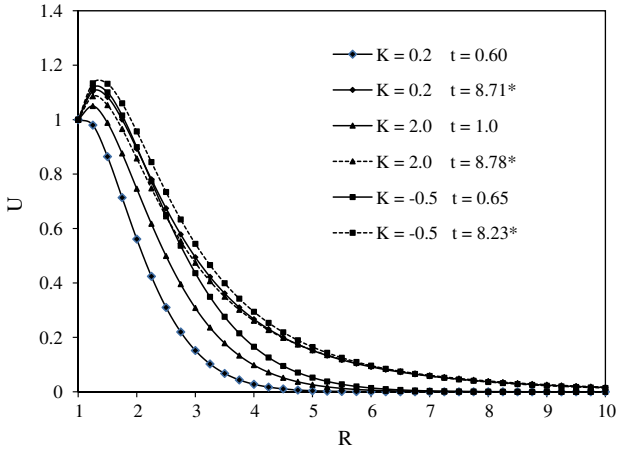

Figure 6 Velocity profiles at $X = 1.0$ for different values of K.

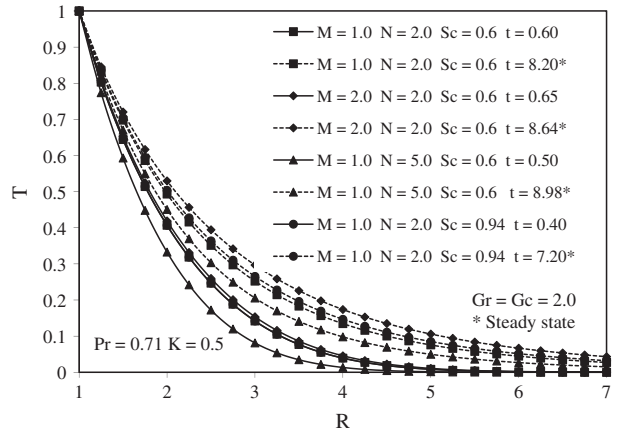

Figure 7 Temperature profiles at $X = 1.0$ for different M, N, and Sc.

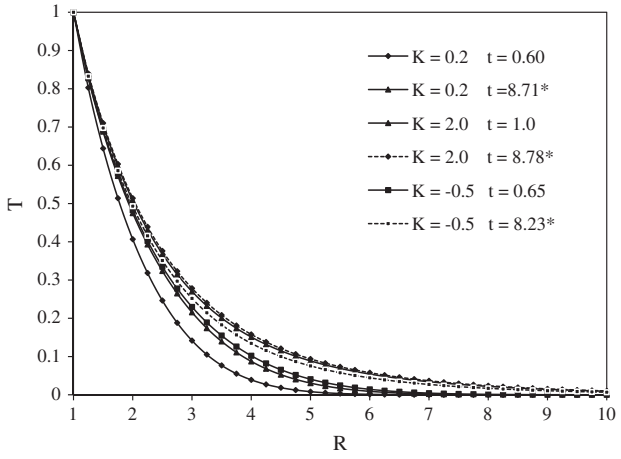

Figure 8 Temperature profiles at $X = 1.0$ for different values of K.

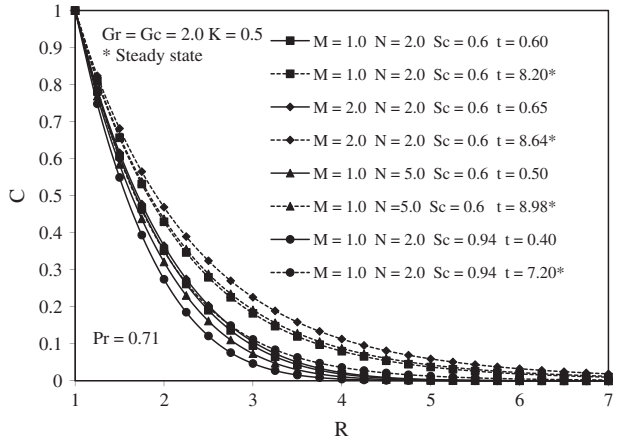

Figure 9 Concentration profiles at $X = 1.0$ for different M, N, and Sc.

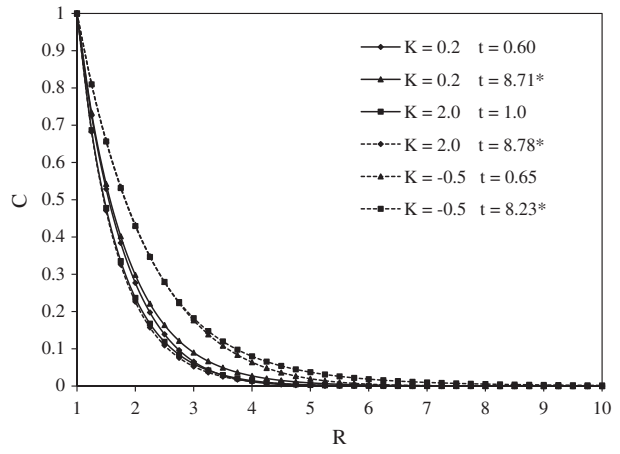

Figure 10 Concentration profiles at $X = 1.0$ for different values of K.

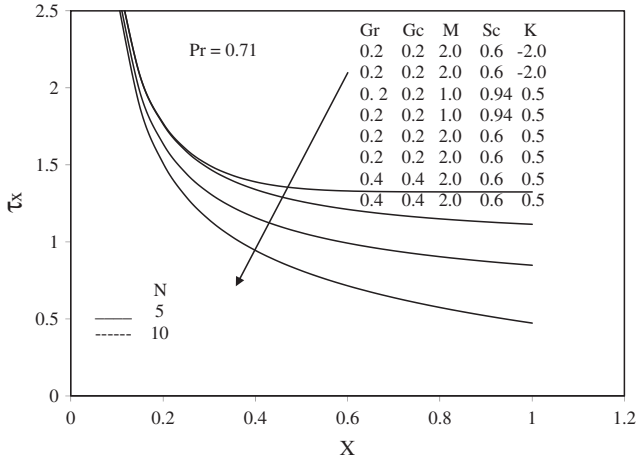

Figure 11 Local skin-friction.

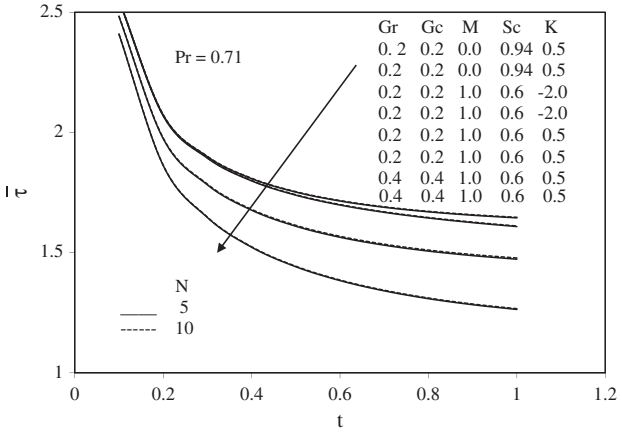

Figure 12 Average skin-friction.

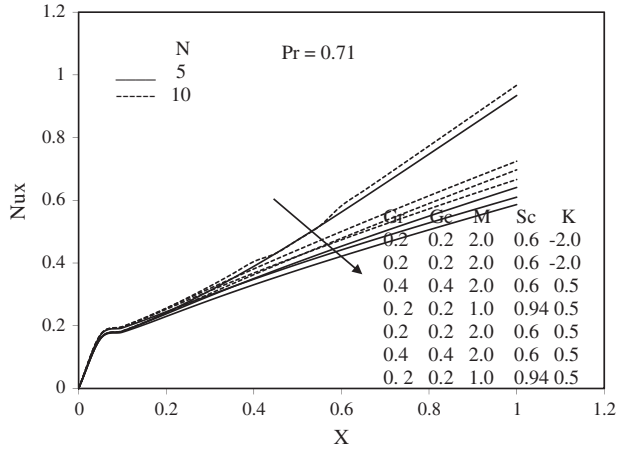

Figure 13 Local Nusselt number.

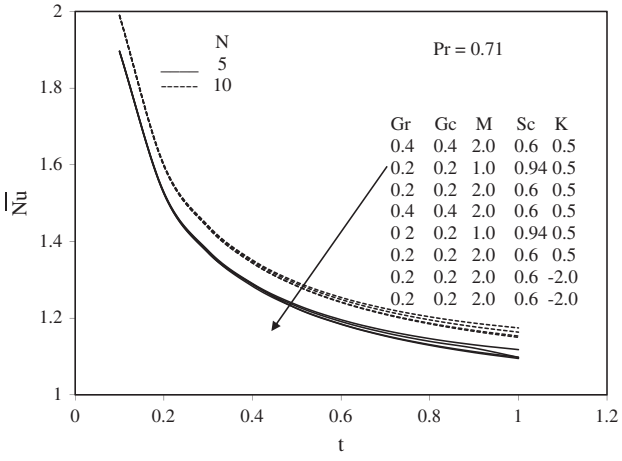

Figure 14 Average Nusselt number.

The transient velocity profiles for different values of Gr, Gc, M, N, Sc, and K at a particular time $t = 0.75$ are shown in Fig. 4. The thermal Grashof number signifies the relative effect of the thermal buoyancy (due to density differences) force to the viscous hydrodynamic force in the boundary layer flow. The positive values of Gr correspond to cooling of the cylinder

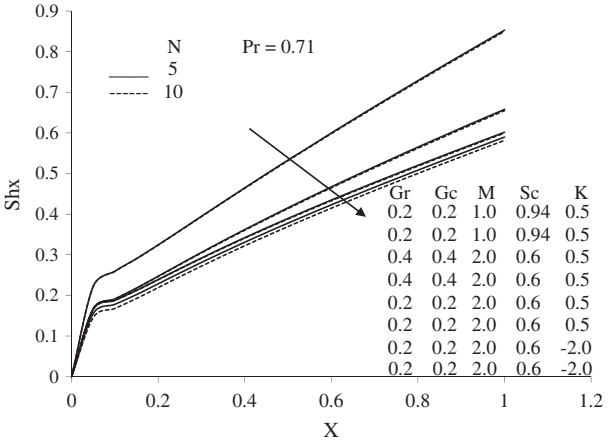

Figure 15 Local Sherwood number.

by natural convection. Heat is therefore conducted away from the vertical cylinder into the fluid which increases temperature and thereby enhances the buoyancy force. It is observed that the transient velocity accelerates due to enhancement in the thermal buoyancy force. The solutal Grashof number *Gc* defines the ratio of the species buoyancy force to the viscous hydrodynamic force. It is noticed that the transient velocity increases considerably with a rise in the species buoyancy force. In both the cases, it is interesting to note that as *Gr* or *Gc* increases, there is rapid rise in the velocity near the surface of vertical cylinder and then descends smoothly to the free stream velocity. As expected, the transient velocity decreases with an increase in the magnetic parameter *M*. It is because that the application of transverse magnetic field will result a resistive type force (Lorentz force) similar to drag force which tends to resist the fluid flow and thus reducing its velocity. Also, the boundary layer thickness decreases with an increase in the magnetic parameter. The radiation parameter *N* (i.e., Stark number) defines the relative contribution of conduction heat transfer to thermal radiation transfer. It can be seen that an in increase in *N* leads to a decrease in the velocity. The Schmidt number *Sc* embodies the ratio of the momentum diffusivity to the mass (species) diffusivity. It physically relates the relative thickness of the hydrodynamic boundary layer and mass-transfer (concentration) boundary layer. It is observed that as the Schmidt number increases, the transient velocity decreases. It is observed that for destructive reaction, increasing values of *K* lead to a fall in velocity profiles.

In Fig. 5, the transient and steady state velocity profiles are presented for different values *Gr*, *Gc*, *M*, *N*, and *Sc*. The steady state velocity increases with an increase in *Gr* or *Gc*. It can be seen that an increase in the thermal or species buoyancy force reduces the time required to reach the steady state. The steady state velocity decreases with an increase in *M* or *N* or *Sc*. The time taken to reach the steady state velocity increases as *M* or *N* increases.

The transient and steady state velocity profiles are presented for different values of *K* is shown in Fig. 6. For the case of $K > 0$, i.e., for destructive reaction, increasing values of *K* lead to a fall in velocity profiles. Time taken to reach steady state increases as *K* increases. A temporal maximum of velocity profiles is clearly seen for decreasing values of *K*. For generative reaction, $K < 0$, a fall in velocity is observed for increasing *K*. This is due to the fact that as $K < 0$, the last term in the momentum equation becomes positive and plays a crucial role. Time required to each steady state increases as *K* decreases. Here, the difference between temporal velocity and steady state velocity is not clear as in the case of $K > 0$.

The transient and steady state temperature profiles are presented for different values *M*, *N*, and *Sc* in Fig. 7. It is observed that, as *N* decreases from 5.0 to 2.0, the temperature increases markedly throughout the length of the cylinder. As a result, the thermal boundary layer thickness is decreasing due to a rise in *N* values. It is noticed that the temperature decreases with an increase in *M* while it increases with an increase in *Sc*. The time required to reach the steady state temperature increases with an increase in *M* or *N* and it decreases with an increase in *Sc*.

In Fig. 8, the transient and steady state temperature profiles are presented for different values of *K*. For generative and destructive reaction, temperature profiles are decreasing as *K* decreases.

In Fig. 9, the transient and steady state concentration profiles are presented for different values of *M*, *N*, and *Sc*. It is found that the concentration decreases as the radiation parameter *N* or the Schmidt number *Sc* increases, while it increases with an increase in *M*. The time required to reach the steady state concentration increases with an increase in *M* or *N* and it decreases with an increase in *Sc*.

The transient and steady state concentration profiles are presented for different values of *K* is shown in Fig. 10. For destructive reaction, as the reaction parameter increases the concentration profiles are decreasing. This is due to the fact that as $K > 0$, the last term in the mass diffusion equation becomes positive and contributes about 50% over the major portion of the profile. A temporal maximum is also observed. It is seen that the temporal maximum is reached at an early stage for increasing *K* and that the profiles differ very much from the steady state profiles. For generative reaction, the opposite effect is observed, i.e., as the reaction parameter increases concentration profiles are thicker. The temporal maximum is attained at an early state for the case of increasing reaction parameter.

Steady state local skin-friction (τ_x) values against the axial coordinate X are plotted in Fig. 11. The local shear stress τ_x increases with an increase in *Sc*, while it decreases with an increase in *Gr* or *Gc* or *M*. The average skin-friction ($\bar{\tau}$) values are shown in Fig. 12. It is found that the average skin-friction increases with an increase in *Sc*, while it decreases with an increase in *Gr* or *Gc* or *M*, throughout the transient period. It is also observed that the average skin-friction increases as the radiation interaction parameter *N* increases. The local Nusselt number (Nu_x) is shown in Fig. 13. The local heat transfer rate decreases with an increase in *Sc*, while it increases with an increase in *Gr* or *Gc* or *M*. Also, it is found that as the radiation parameter *N* increases, the local Nusselt number increases. The average Nusselt number ($\overline{Nu}$) values are shown in Fig. 14. It is observed that the average Nusselt number increases with an increase in *Gr* or *Gc* or *N*. The local Sherwood number Sh_X is plotted in Fig. 15. It is noticed that Sh_X increases with an increase in *Sc*, where as it decreases with an increase in *Gr* or *Gc* or *N*. The average Sherwood number ($\overline{Sh}$) values are shown in Fig. 16. It can be seen that the average Sherwood number increases with an increase in *Gr* or *Gc* or *Sc*, while it decreases with an increase in *M*.

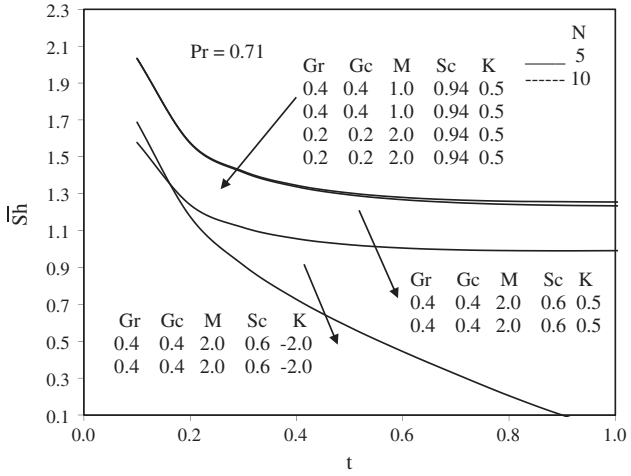

Figure 16 Average Sherwood number.

5. Conclusions

The interaction of free convection chemically reactive species and thermal radiation of a viscous incompressible unsteady MHD flow past a moving vertical cylinder is studied numerically. The fluid is gray, absorbing-emitting but non-scattering medium and the Rosseland approximation is used to describe the radiative heat flux in the energy equation. A family of governing partial differential equations is solved by an implicit finite difference scheme of Crank–Nicolson type, which is stable and convergent. The conclusions of this study are as follows:

1. The transient velocity increases with an increase in *Gr* or *Gc*.
2. As the magnetic field parameter *M* increases, the transient velocity decreases.
3. At small values of the radiation parameter *N*, the velocity and temperature of the fluid increases sharply near the cylinder as the time t increase.
4. For generative reaction, as the reaction constant increases, velocity and concentration are found to be decreasing and temperature is increasing. For destructive reaction, as the reaction constant decreases, velocity and concentration increase and temperature decreases.
5. The local and average skin-friction $\bar{\tau}$ decreases with an increase *M* and increases with increasing value of *N* and *Sc*.
6. The average Nusselt number $\overline{Nu}$ increases with increasing value of radiation parameter *N* and decreasing values of *Sc*.
7. The Sherwood number $\overline{Sh}$ increases as *Sc* increases.

References

[1] Evan LB, Reid RC, Drake EM. Transient natural convection in a vertical cylinder. AIChE J 1968;14:251–61.
[2] Velusamy K, Garg VK. Transient natural convection over a heat generating vertical cylinder. Int J Heat Mass Transfer 1992;35:1293–306.
[3] Michiyoshi I, Takahashi I, Seizawa A. Natural convection heat transfer form a horizontal cylinder to mercury under a magnetic field. Int J Heat Mass Transfer 1976;19:1021–9.
[4] Ganesan P, Loganathan P. Magnetic field effect on a moving vertical cylinder with constant heat flux. Heat Mass Transfer 2003;39:381–6.
[5] Gnaneswara Reddy M, Bhaskar reddy N, Ramakrishna Reddy B. Unsteady MHD convective heat and mass transfer flow past a semi-infinite vertical porous plate with variable viscosity and thermal conductivity. Int J Appl Math Mech 2009;b(6):1–14.
[6] Chen TS, Yuh CF. Combined heat and mass transfer in natural convection along a vertical cylinder. Int J Heat Mass Transfer 1980;23:451–61.
[7] Takhar HS, Chamkha AJ, Nath G. Combined heat and mass transfer along a vertical cylinder with free stream. Heat Mass Transfer 2000;36:237–46.
[8] Ganesan P, Loganathan P. Unsteady free convection flow over a moving vertical cylinder with heat and mass transfer. Heat Mass Transfer 2001;37(1):59–65.
[9] Ganesan P, Rani HP. Transient natural convection cylinder with heat and mass transfer. Heat Mass Transfer 1998;33:449–55.
[10] Shanker B, Kishan N. The effects of mass transfer on the MHD flow past an impulsively started infinite vertical plate with variable temperature or constant heat flux. J Eng Heat Mass Transfer 1997;19:273–8.
[11] Ganesan P, Rani HP. Unsteady free convection MHD flow past a vertical cylinder with heat and mass transfer. Int J Therm Sci 2000;39:265–72.
[12] Gnaneswara Reddy M. Unsteady free convective flow past a semi-infinite vertical plate with uniform heat and mass flux. J Petrol Gas Explor Res 2012;2(3):052–6.
[13] Arpaci VS. Effects of thermal radiation on the laminar free convection from a heated vertical plate. Int J Heat Mass Transfer 1968;11:871–81.
[14] Cess RD. Interaction of thermal radiation with free convection heat transfer. Int J Heat Mass Transfer 1966;9:1269–77.
[15] Cheng EH, Ozisik MN. Radiation with free convection in an absorbing emitting and scattering medium. Int J Heat Mass Transfer 1972;15:1243–52.
[16] Raptis A. Radiation and free convection flow through a porous medium. Int Commun Heat Mass Transfer 1998;25(2):289–95.
[17] Hossain MA, Takhar HS. Radiation effects on mixed convection along a vertical plate with uniform surface temperature. Heat Mass Transfer 1996;31:243–8.
[18] Hossain MA, Takhar HS. Thermal radiation effects on the natural convection flow over an isothermal horizontal plate. Heat Mass Transfer 1999;35:321–6.
[19] Das UN, Deka R, Soundalgekar VM. Radiation effects on flow past an impulsively started vertical plate-an exact solutions. J Theor Appl Fluid Mech 1996;1(2):111–5.
[20] Yih KA. Radiation effects on natural convection over a vertical cylinder embedded in porous media. Int Commun Heat Mass Transfer 1999;26(2):259–67.
[21] Ganesan P, Loganathan P. Radiation and mass transfer effects on flow of an incompressible viscous fluid past a moving vertical cylinder. Int J Heat Mass Transfer 2002;45:4281–8.
[22] Gnaneswara Reddy M, Reddy Bhaskar. Radiation and mass transfer effects on unsteady MHD free convection flow past a moving vertical cylinder. Theor Appl Mech 2009;36(3):239–60.
[23] Gnaneswara Reddy M, Bhaskar Reddy N. Thermal radiation and mass transfer effects on MHD free convection flow past a vertical cylinder with variable surface temperature and concentration. J Naval Archit Mar Eng 2009;6:1–15.
[24] Makinde OD. Chemically reacting hydromagnetic unsteady flow of a radiating fluid past a vertical plate with constant heat flux. Z Naturforsch 2012;67a:239–47.
[25] Makinde OD. MHD mixed-convection interaction with thermal radiation and *n*th order chemical reaction past a vertical porous plate embedded in a porous medium. Chem Eng Commun 2011;198(4):590–608.

[26] Ibrahim SY, Makinde OD. Radiation effect on chemically reacting MHD boundary layer flow of heat and mass transfer past a porous vertical flat plate 2011;6(6):1508–16.
[27] Brewster MQ. Thermal radiative transfer and properties. New York: John Wiley & Sons; 1992.
[28] Carnahan B, Luther HA, Wilkes JO. Applied numerical methods. New York: John Wiley & Sons; 1969.
[29] Richtmyer RobertD, Morton KW. Difference methods for initial – value problems. New York: John Wiley & Sons; 1967.

Gnaneswara Reddy Machireddy was born and brought up in Chittoor District, Andhra Pradesh. He obtained the B.Sc. Computers and M.Sc. degrees in Mathematics from the Sri Venkateswara University, Tirupati. He joined as a regular research scholar in the Department of Mathematics, the Sri Venkateswara University in 2006 and was awarded his Ph.D. degree in Fluid Mechanics from the same University in 2009. He is working as an Assistant Professor in the Department of Mathematics, Acharya Nagarjuna University, Andhra Pradesh since 2009. His research interest covers the areas are convection flows, heat transfer and mass transfer in porous/non-porous media. His research interest also covers applied cryptography.